Anat Embryol (2001) 204:319–332

ORIGINAL ARTICLE

Asgeir Brevik · Trygve B. Leergaard
Marius Svanevik · Jan G. Bjaalie

Three-dimensional computerised atlas of the rat brain stem precerebellar system: approaches for mapping, visualization, and comparison of spatial distribution data

Accepted: 14 June 2001

Abstract Comparisons of microscopical neuroanatomic data from different experiments and investigators are typically hampered by the use of different section planes and dissimilar techniques for data documentation. We have developed a framework for visualization and comparison of section-based, spatial distribution data, in brain stem nuclei. This framework provides opportunities for harmonized data presentation in neuroinformatics databases. Three-dimensional computerized reconstructions of the rat brain stem and precerebellar nuclei served as a basis for establishing internal coordinate systems for the pontine nuclei and the precerebellar divisions of the sensory trigeminal nuclei. Coordinate based diagrams were used for presentation of experimental data (spatial distribution of labelled neurons and axonal plexuses) from standard angles of view. Each nuclear coordinate system was based on a cuboid bounding box with a defined orientation. The bounding box was size-adjusted to touch cyto- and myeloarchitectonically defined boundaries of the individual nuclei, or easily identifiable nearby landmarks. We exemplify the use of these internal coordinate systems with dual retrograde neural tracing data from pontocerebellar and trigeminocerebellar systems. The new experimental data were combined, in the same coordinate based diagrams, with previously published data made available via a neuroinformatics data repository (www.nesys.uio.no/Database, see also www.cerebellum.org). Three-dimensional atlasing, internal nuclear coordinate systems, and consistent formats for presentation of neuroanatomic data in web-based data repositories, offer new opportunities for efficient analysis and re-analysis of neuroanatomic data.

A. Brevik · T.B. Leergaard · M. Svanevik · J.G. Bjaalie (✉)
Department of Anatomy, Institute of Basic Medical Sciences, University of Oslo, P.O. Box 1105 Blindern, N-0317, Oslo, Norway
e-mail: j.g.bjaalie@basalmed.uio.no
URL: http://www.nesys.uio.no/
Tel.: +47-22-851263

Keywords 3-D reconstruction · Brain template · Cerebellum · Pontine nuclei · Trigeminal sensory nuclei · Coordinate system · Retrograde tracing

Introduction

The structural organization of the brain and its circuitry is commonly studied with neural tracing techniques. Increasingly sensitive tracer substances are used to characterize the terminal fields (targets) of particular populations of projection neurons (anterograde tracing), or to trace the cells of origin (sources) of afferent nerve fibres to a particular target zone (retrograde tracing, see, e.g. Glover et al. 1986; Köbbert et al. 2000; Reiner et al. 2000). Furthermore, new trans-synaptic viral tracing techniques are employed to trace multiple (synaptically interrupted) links in neural circuits (Ugolini 1995; Tang et al. 1999; Middleton and Strick 2001). While these refined techniques offer new and unique possibilities for mapping wiring patterns in the brain, data obtained in different laboratories are often difficult to compare. Comparisons of results are typically hampered by variation in the resolution of drawings or photomicrographs, the plane of sectioning, the use of different section spacing, and dissimilar techniques for data documentation. These problems are common to most anatomic brain mapping investigations (Swanson 1995, 2000; Toga and Mazziotta 1996; Schmahmann et al. 1999; Thompson et al. 1997; Toga and Thompson 1999; Thompson et al. 2000; Geyer et al. 2001; Toga et al. 2001). Furthermore, the traditional data formats (journal figures) are inefficient for re-analysis of previously published results. Inspired by recent developments in the field of databasing and data sharing (Chicurel 2000; Koslow 2000; Swanson 2000; Svanevik et al. 2000), we have explored new approaches for effective presentation of anatomic data, suitable for comparison and re-use of data across laboratories.

The present study is related to our ongoing investigations of mossy fibre pathways to the somatosensory

influenced regions of the cerebellar hemispheres (Leergaard et al. 1995 2000a,b; Thompson et al. 1995; Bjaalie et al. 1997b; Hallem et al. 1999; Vassbø et al. 1999; Svanevik et al. 2000; De Schutter and Bjaalie 2001). We have focussed on precerebellar brain stem systems (for review, see Newman and Ginsberg 1992; Ruigrok and Cella 1995; Voogd 1995) and have made computerised three-dimensional (3-D) reconstructions of the brain stem and several precerebellar nuclei in the rat. Based on the 3-D reconstructions we have established internal coordinate systems and standard diagrams for the presentation of results for the pontine nuclei and trigeminal sensory nuclei. We exemplify the use of the internal coordinate systems and nuclear diagrams by mapping the distribution of pontocerebellar and trigeminocerebellar neurons labelled following deposition of tracers into defined parts of the cerebellar hemispheres. Furthermore, we combine our new experimental data with previously published data made available via a neuroinformatics data repository (http://www.nesys.uio.no/ and http://www.cerebellum.org/).

Materials and methods

Four adult female Sprague Dawley rats with body weight from 240 g to 280 g were used. Two animals were used as a basis for a computerised 3-D reconstruction of the normal brain stem and cerebellum. The remaining animals were used for retrograde tracing experiments. All animal procedures were approved by an institutional animal welfare committee and were in compliance with national laws and with National Institutes of Health guidelines for the use and care of laboratory animals. Previously published experimental data (Leergaard et al. 2000b) were downloaded from http://www.nesys.uio.no/Database/.

Surgical procedures, tracer implantations, and histological processing

The animals were anesthetised by subcutaneous injection of 3 ml/kg of a mixture of equal volumes of Hypnorm (fentanyl citrate 0.315 mg/ml and fluanisone 10 mg/ml, Janssen, High Wycombe, UK) and Dormicum (midazolam 5 mg/ml, Hoffmann-La Roche, Basel, Switzerland). Surgical anesthesia was defined by absence of response to external stimuli (of cornea, ears, tail, and perioral area).

Normal material

To obtain normal material for histological processing, two animals (R201 and R202) were perfused transcardially with lukewarm saline followed by 4% paraformaldehyde and 10% sucrose. The brains were removed and stored in 30% sucrose for 1 to 5 days. All solutions were phosphate-buffered. The brain stems with cerebelli were embedded in 9% phosphate-buffered gelatine and serial sections were cut at 50 µm on a freezing microtome. One brain used as normal material was cut transversely (R201), the other sagittally (R202). The transverse section plane was here defined as perpendicular to the baseline of the rat brain, placed on a horizontal surface. This section plane was estimated to deviate 7–8° from the frontal plane used by Paxinos and Watson (1998), and was chosen to ensure reproducible section planes (Fig. 1). Every third section was stained with the Woelcke method for myelin (Woelcke 1942) combined with cresyl-violet cell staining. All remaining sections were stained with cresyl-violet.

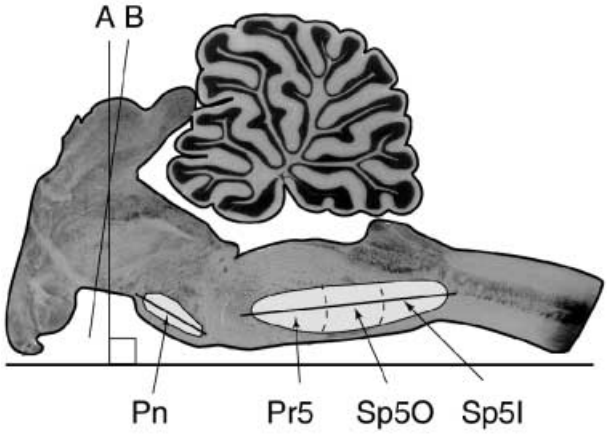

Fig. 1 Photomicrograph of a Woelcke- and cresyl violet stained sagittal section from a level 1 mm lateral to the midline. Line *A* indicates the transverse section plane used in the present study, defined as perpendicular to the baseline of the rat brain placed on a horizontal surface. Line *B* indicates the frontal section plane used by Paxinos and Watson (1998). The longitudinal axes of the brain stem at level of the pontine nuclei and the trigeminal sensory nuclei are indicated by lines. The internal coordinate systems were aligned along the longitudinal axes (*Pn* pontine nuclei; *Pr5* principal sensory trigeminal nucleus; *Sp5I* spinal trigeminal nucleus, interpolar part; *Sp5O* spinal trigeminal nucleus, oral part)

Experimental material

For the retrograde tracing experiments (R203 and R204), the head was immobilised in a stereotaxic frame, and a small opening (~ 2×4 mm) was made in the cranium overlying the cerebellar cortex. Small crystals (diameter of 350–450 µm) of dextran amine conjugated with rhodamine (FluoroRuby FR, Molecular Probes, Eugene, Ore) and fluorescein (FluoroEmerald, FE, Molecular Probes) were implanted in the cerebellar cortex using the method described by Glover (1995). In both experiments, FR was implanted in the crown of crus IIa (aimed at the large upper lip-related representation, using vascular patterns as guidance, cf. Bower and Kassel, 1990; Hallem et al. 1999), while FE was placed either more medially in crus IIa (case 203) or in the crown of the adjacent folium crus I (case 204). The cranial opening was rinsed with saline and covered with subcutaneous muscle before the skin was sutured. After a survival period of 7 days, the animals were reanesthetised and perfused as described above. The two experimental brains were cut transversely (Fig. 1). In case R204, every second section through the cerebellar tracer implantation site was incubated with monoclonal antibodies raised against zebrin II (Hawkes and Leclerc 1986). The avidin-biotin-peroxidase complex method of Lehre et al. (1995) was used to identify the distribution of anti-zebrin II labelling in crus IIa (for further details, see Hallem et al. 1999). The localisation of the tracer implantation was defined in relation to the zebrin pattern in crus I and IIa, and compared to available maps on the correspondence between zebrin patterns and electrophysiologically defined representations (Hallem et al. 1999).

Data acquisition

Structures of interest were digitised as contour lines or point coordinates (Fig. 2), using an image-combining computerised microscope system, based on the Leica DMR microscope equipped with Leitz Plan Fluotar ×10 and ×20 lenses. Details on software and technical solutions have been reported in Leergaard and Bjaalie (1995).

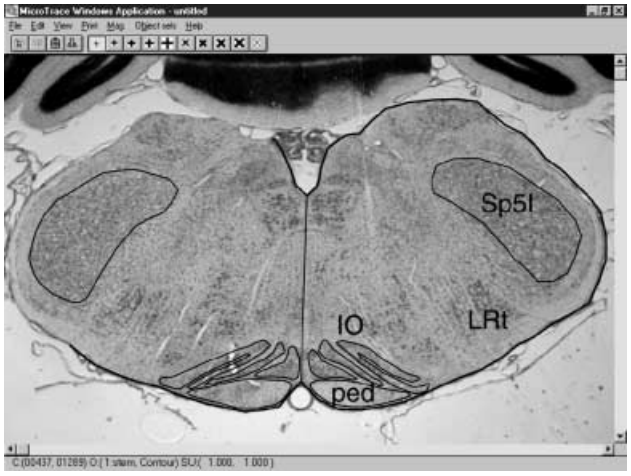

Fig. 2 The graphical interface of the data acquisition programme MicroTrace (Leergaard and Bjaalie, 1995): field of view in the image-combining computerized microscope. The specimen is a transverse section through the medulla oblongata at level of the inferior olive, stained for cresyl-violet. The outline contours of the brain stem and the peduncle, as well as the nuclear boundaries of the trigeminal sensory nuclei and the inferior olive, are digitised as lines (*IO* inferior olive; *LRt* lateral reticular nucleus; *ped*, peduncle; *Sp5I* spinal trigeminal nucleus, interpolar part)

Normal series

The two normal series of sections were viewed with translucent light. Differential interphase contrast was used to facilitate the visualization of nuclear boundaries and other landmarks. From the *transverse* normal sections (case R201), the outlines of the pontine nuclei, the reticulotegmental nucleus of the pons, the trigeminal sensory nuclei, the lateral reticular nucleus, and the inferior olive, were digitised as contour lines in every third section, along with surface contour lines of the brain stem and cerebellum, the contours of the corticobulbar and corticospinal fibre tracts (in the following referred to as the peduncle), the midline, and the outlines of the fourth ventricle. Boundaries of nuclei and fibre tracts were identified according to conventional myeloarchitectonic and cytoarchitectonic criteria (reviewed by Newman and Ginsberg 1992; Ruigrok and Cella 1995; Voogd 1995; Waite and Tracey 1995) as exemplified in Fig. 3. For the lateral reticular nucleus, all cresyl-violet-stained cell bodies, judged as belonging to this nucleus, were digitised as point coordinates in every third section, and used to define nuclear boundaries.

Experimental series

The two experimental series of sections were viewed with the fluorescence unit, using excitation light of 515–560 nm (Leitz N2.1 filter block) to visualize FR labelling, excitation light of 480 nm (Leitz L5 filter block) to visualize FE labelling, and excitation light of 490 nm (Leitz FI/RH filter block) dual filter for simultaneous visualization of FR and FE labelling. Anatomic landmarks were recognised by differences in auto-fluorescence observed through the UV filter (Leitz A filter block). In the sections containing labelled neurons anatomic landmarks were digitised as contour lines as described above. Labelled neurons were coded as point coordinates, in three categories as neurons labelled with FR, FE, or both.

3-D reconstruction

For computerised 3-D reconstruction, the digitised data were transferred to Silicon Graphics workstations running software Micro3D (version 2000; Oslo Research Park, Oslo, Norway), developed in our laboratory (http://www.nesys.no) and used in several recent investigations (Leergaard et al. 1995 2000a,b; Malmierca et al. 1995, 1998; Bjaalie et al. 1997a, b; Berg et al. 1998, 1999; Vassbø et al. 1999). The digitised sections were assigned z-values defined by section thickness and serial numbers, before they were aligned interactively on the screen with the aid of multiple anatomic landmarks. The initial alignment of *transverse* brain stem sections was based on alignment of reference lines (midline, fourth ventricle, peduncle, and others) as well as rotation and inspection of the reconstruction from various angles of view. Digitised *sagittal* sections from one of the normal brains were used as templates for the fine dorsoventral adjustment of the sections (Fig. 4). The outer surface of the right cerebellum was reconstructed by combined alignment of transverse and sagittal sections. The cerebellar reconstruction shown in Figures 5 and 7 was based on sagittal sections. The left half of the reconstruction is a mirror copy of the right half. Tissue shrinkage was estimated for all sections by comparing drawings of sections before and after histochemical processing. To maintain correct in-vivo proportions, those reconstructions that were based on myelin or cresyl-violet stained sections were size adjusted in the x,y plane to correct for 5% tissue shrinkage. Surface modeling was performed with the use of the software library SISL (SINTEF Spline Library; cf. Bjaalie et al. 1997a).

The overall distribution of labelling in the pontine and trigeminal nuclei was studied with real-time rotations on the computer screen and shown in standard angles of view (Figs. 5A–C, 6, 8). To facilitate inspection of the distribution pattern from an angle of view perpendicular to the plane of sectioning, the z-values of point-coded data were randomised within the range of their respective section spacing (Figs. 6, 8). The distribution patterns were analysed at higher detail in series of slices through the 3-D reconstructions (section planes at chosen angles of orientation). Section-independent subdivisions, or slices, through a reconstruction were useful for demonstrating additional features of the labelling pattern (Fig. 8H–M; see also Leergaard et al. 2000a,b.)

File formats

The experimental data produced in the present study were combined with previously published data downloaded from a neuroinformatics data repository (http://www.nesys.uio.no/Database/). Both the new and the previously published data were available in the same Micro3D file formats (modified inventor format, and simple XYZ coordinate files), that can be readily converted to more frequently used file formats, e.g. the MBF ascii format of Neurolucida (MicroBrightField, Colchester, VT).

Assembly of illustrations

Photomicrographs were obtained through a Nikon Multiphot microscope (Nikon, Tokyo, Japan) equipped with a MacroNIKKOR 1:4.5 lens (Figs. 1, 2, 4), or with a CoolSnap digital camera (Photometrics, Tuzon, AZ) through a Leica DMR microscope (Fig. 3). Illustrations were assembled with Showcase (Silicon Graphics, Mountain View, Calif.), Adobe Illustrator 8.0, and Adobe Photoshop 5.5. The grey-scale levels of the images were optimised using the “curves” function for “autolevels” in Adobe Photoshop.

Results

Our 3-D reconstruction of the normal brain stem precerebellar nuclei includes the pontine nuclei, the precerebellar division of the trigeminal sensory nuclei, the reticulotegmental nucleus of the pons, the lateral reticular nucleus, and the inferior olive. Other quantitatively minor pre-

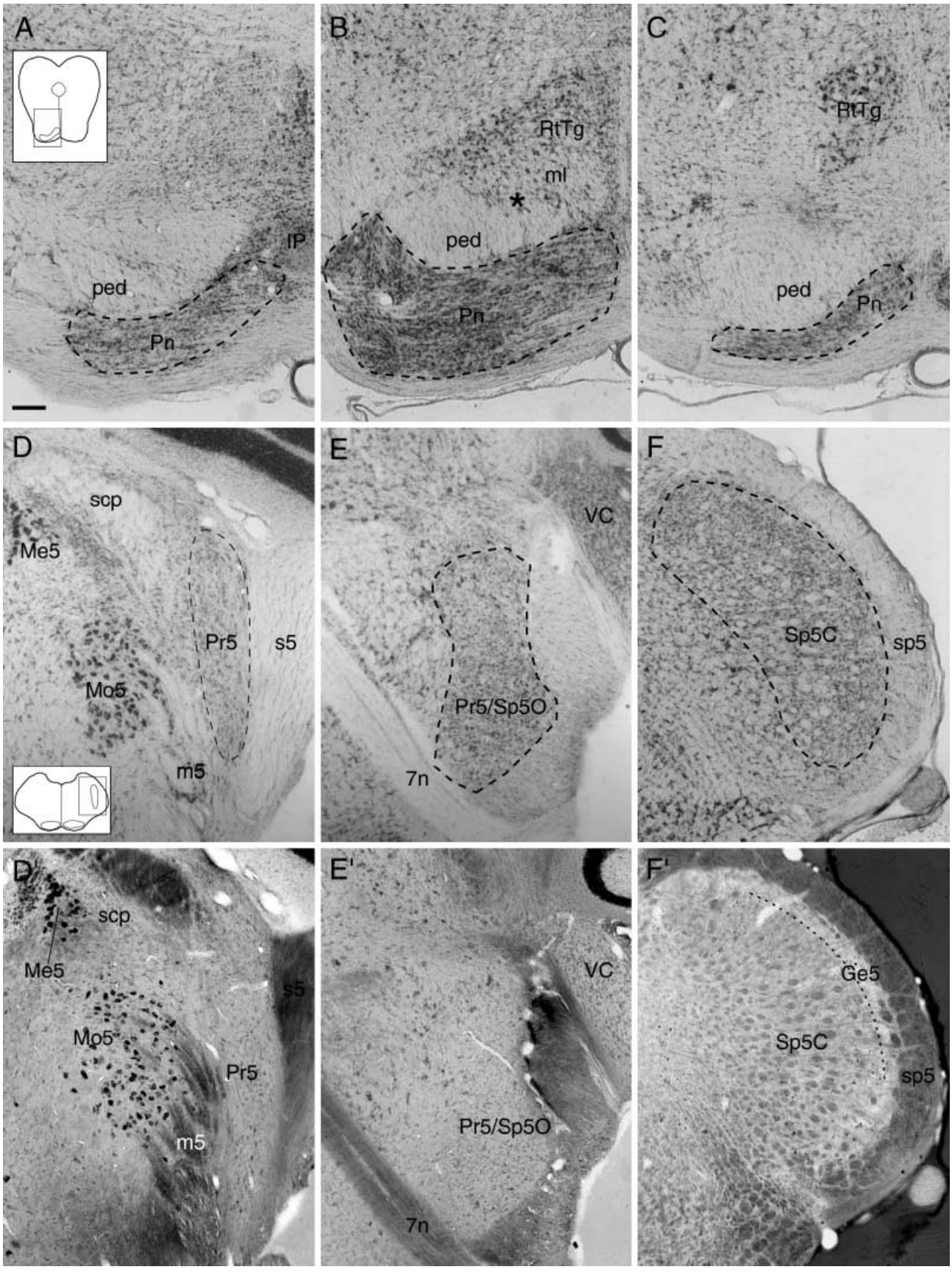
A
IP
ped
Pn
B
RtTg
ml
*
ped
Pn
C
RtTg
ped
Pn
D
scp
Me5
Pr5
s5
Mo5
m5
E
VC
Pr5/Sp5O
7n
F
Sp5C
sp5
D'
scp
Me5
s5
Mo5
Pr5
m5
E'
VC
Pr5/Sp5O
7n
F'
Ge5
Sp5C
sp5

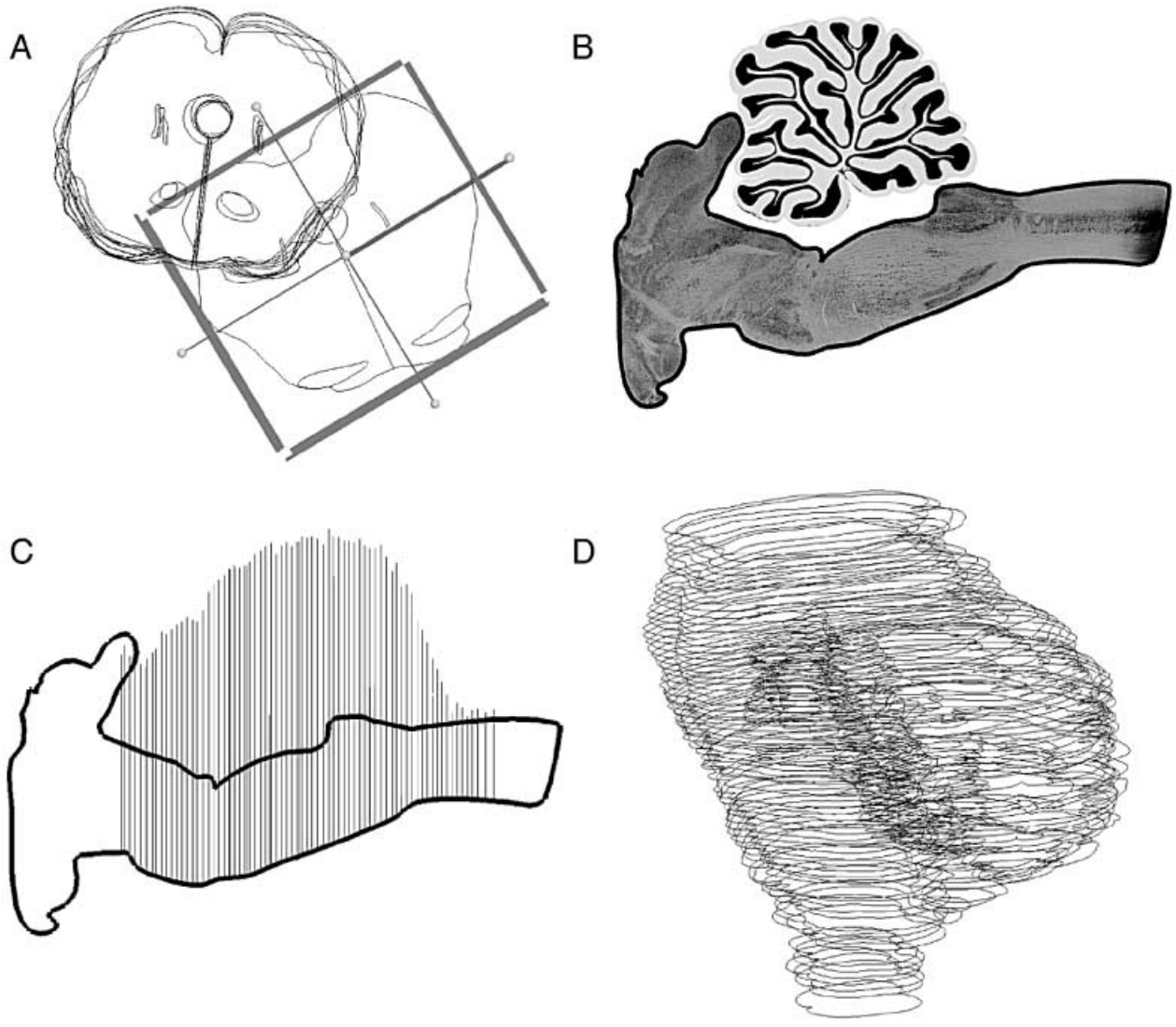

Fig. 4A–D Assembly and visualisation of a 3-D reconstruction of the brain stem and cerebellum. **A** Series of digitised transverse brain stem sections are aligned according to multiple anatomic landmarks. **B** Photomicrograph of a Woelcke- and cresyl violet stained sagittal section from a level 1 mm lateral of the midline. The outline contours of the brain stem are digitised, and in **C** combined with the 3-D reconstruction for fine adjustment of the dorsoventral alignment of the transverse sections. **D** Oblique lateral view of the complete aligned 3-D reconstruction. Real-time rotation with inspection of the 3-D reconstruction from different angles of view was used to facilitate alignment

cerebellar nuclei, such as the paramedian reticular nucleus and the perihypoglossal nuclei (Brodal 1981), were not reconstructed. In this report we have applied nomenclature as used by Ruigrok and Cella (1995), Waite and Tracey (1995), and Paxinos and Watson (1998). Nuclear boundaries were identified on the basis of cyto- and myeloarchitectonic criteria. To facilitate accurate 3-D data presentation and inter-individual comparison of distribution data, we here present internal coordinate sys-

◀ **Fig. 3** Photomicrographs of three transverse sections through the pontine nuclei (**A–C**), and three pairs of adjacent transverse sections through the trigeminal sensory nuclei (**D–F** and **D'–F'**). The sections were stained with cresyl violet (**A–C** and **D–F**), or with the Woelcke method for myelin combined with cresyl violet (**D'–F'**). **A**, **B**, and **C** are from rostral, intermediate and caudal levels of the pontine nuclei, respectively. **D** and **D'** are from a level close to the rostral cap of the trigeminal sensory nuclei. **E** and **E'** are approximately from the level of transition from Pr5 to Sp5O. **F** and **F'** are from a level in the rostral end of Sp5C, close to the caudal border of Sp5I. The presence of the gelatinous layer of Sp5C along the lateral border of sp5 indicates that Sp5I is not present at this level. The first section (from caudal) in which this phenomenon is observed is used to define the caudal border of Sp5I. Nuclear borders are identified on the basis on cytoarchitectonic and myeloarchitectonic criteria. The cellular area of the pontine nuclei (main ventral part) and the sensory trigeminal nuclei are indicated by dotted lines in **A–C** and **D–F**, respectively. Small cell groups belonging to the pontine nuclei are also found inside the peduncle and along its dorsal aspect (**B**, *asterisk*). (*7n*, facial nerve, root; *Ge5* gelatinous layer of Sp5C; *m5* trigeminal nerve, motor root; *IP* interpeduncular nuclei; *Me5* mesencephalic trigeminal nucleus; *ml* medial lemniscus; *Mo5* motor trigeminal nucleus; *ped* peduncle; *Pn* pontine nuclei; *Pr5* principal sensory trigeminal nucleus; *RtTg* reticulotegmental nucleus of the pons; *s5* trigeminal nerve, sensory root; *scp* superior cerebellar peduncle; *sp5* spino trigeminal tract; *Sp5C* spinal trigeminal nucleus, caudal part; *Sp5O* spinal trigeminal nucleus, oral part; *VC* ventral cochlear nucleus *Bar* 200 µm

tems for the pontine nuclei and trigeminal sensory nuclei and exemplify their use with retrograde tracing data.

Definition of pontine nuclei and precerebellar trigeminal sensory nuclei

The term pontine nuclei is here used to include the grey matter partly embracing the descending fibre tract (corticobulbar and corticospinal fibres, referred to as the peduncle) and the medial lemniscus (Fig. 3A–C) at the level of the pons (Mihailoff et al. 1981, 1985; Wiesendanger and Wiesendanger 1982; Panto et al. 1995; Leergaard et al. 2000a,b; for a review, see Ruigrok and Cella 1995). We consider the reticulotegmental nucleus as independent from the pontine nuclei, since it is differently organised with respect to cytoarchitecture and connectivity (Mihailoff et al. 1981; Torigoe et al. 1986; Ruigrok and Cella 1995; see, however, Schwarz and Thier 1996). Our 3-D reconstructions outline the boundaries of the main part of the pontine nuclei (shown in red, Fig. 5), located between the ventral surface and the peduncle. These boundaries were readily identified in the cresyl-violet-stained sections, and in unstained sections, using, e.g., differential interphase contrast microscopy.

The term precerebellar trigeminal sensory nuclei is here used to include the principal sensory trigeminal nucleus (Pr5) and the oral (Sp5O) and interpolar (Sp5I) parts of the spinal trigeminal nucleus (Fig. 1), which are the known sources of cerebellar afferents (Newman and Ginsberg 1992; for review, see Waite and Tracey 1995). These three divisions form a continuous, rostrocaudally elongated, structure. At the rostral end, the Pr5 is located close to the trigeminal motor nucleus (Fig. 3 D and D'), intercalated between the motor and sensory roots of the trigeminal nerve. The Pr5 extends dorsally towards the Kölliker-Fuse nucleus, situated adjacent to the superior cerebellar peduncle. At the caudal end, the Sp5I is separated from a neighbouring caudal part of the trigeminal nuclei (the caudal spinal trigeminal nucleus, Sp5C) by the obliquely oriented gelatinous layer of the Sp5C. This layer is visible in sections stained for myelin (Fig. 3F') or cytochrome oxidase (Phelan and Falls 1989). The lateral boundaries of the trigeminal sensory nuclei are readily distinguished from the adjacent white matter, whereas the medial boundaries are less sharply defined (Fig. 3D–F, D'–F'). The location and shape of the precerebellar trigeminal sensory nuclei and its continuation, the Sp5C, is shown to advantage in the 3-D reconstruction (Fig. 5).

Internal coordinate system for the pontine nuclei

The internal coordinate system for the pontine nuclei was established by introducing a cuboid bounding box oriented perpendicular to the midsagittal plane, and parallel with the ventral surface of the descending fibre tracts, the peduncles. Thus, the bounding box was oriented along the long axis of the brain stem at the level at the pons (Fig. 1). Using cytoarchitectonic criteria, the bounding box was size-adjusted to touch the rostral, caudal, medial, lateral, and ventral ends of the pontine nuclei (Figs. 6D, 7). The rostral and caudal boundaries were unambiguously defined by the presence of grey substance ventral to the descending fibre tract. Similarly, the lateral and ventral extents of the pontine nuclei (i.e. grey matter) were readily seen also in unstained sections, e.g., with the use of differential interphase contrast or autofluorescence. The dorsal end of the pontine nuclei was, however, more difficult to define cytoarchitectonically. We therefore chose to use the ventral surface of the peduncle as an intermediate landmark for defining the dorsal limit of the bounding box. Thus, we placed the centre-point of the bounding box at the ventral surface of the peduncle, halfway from rostral to caudal, and halfway from the midline to the lateral end of the pontine nuclei (Fig. 6, see arrow in Fig. 7). The distance from the centre-point to the dorsal end of the bounding box was set to be equal to the distance from the centre-point to the ventral limit of the bounding box.

The origin of the internal coordinate system was defined as the intersection of the three planes formed by the medial and rostral sides of the bounding box, and the plane halfway from ventral to dorsal (through the above defined centre-point, Figs. 6D, 7). Relative coordinates from 0 to 100% were defined from rostral to caudal, medial to lateral, and from 'central' (the plane halfway from ventral to dorsal) to ventral (100%) and dorsal (-100%) within the pontine nuclei (Figs. 6, 7). To facilitate presentation and comparison of distribution data, separate diagrams for standard ventral, lateral and rostral angles of view, were used (Fig. 6D, E, 8A–C; Leergaard et al. 2000a,b, see also http://www.nesys.uio.no/Database). By subdividing the 3-D reconstructions into slices of a chosen thickness and orientation, it was furthermore possible to study topographic distribution patterns in greater detail and independently of the original section plane (Leergaard et al. 2000a,b). Different angles of view and slicing are needed to demonstrate complex distributions throughout the pontine nuclei.

Internal coordinate system for precerebellar trigeminal sensory nuclei

A similar internal coordinate system, divided into relative values from 0 to 100%, and with accompanying diagrams for visualization (Fig. 6F, G), was designed for the precerebellar trigeminal sensory nuclei (the Pr5, Sp5O, and Sp5I, Newman and Ginsberg 1992). Again, a cuboid bounding box was oriented perpendicular to the midsagittal plane. Furt her, the bounding box was oriented along the long axis of the nuclear complex (Fig. 1) and size adjusted to touch the lateral, ventral, and dorsal ends of the nuclear complex (Fig. 6F,G). The lateral boundary was defined by the transition from grey matter (trigeminal nuclei) to white matter (spinal trigeminal tract). The

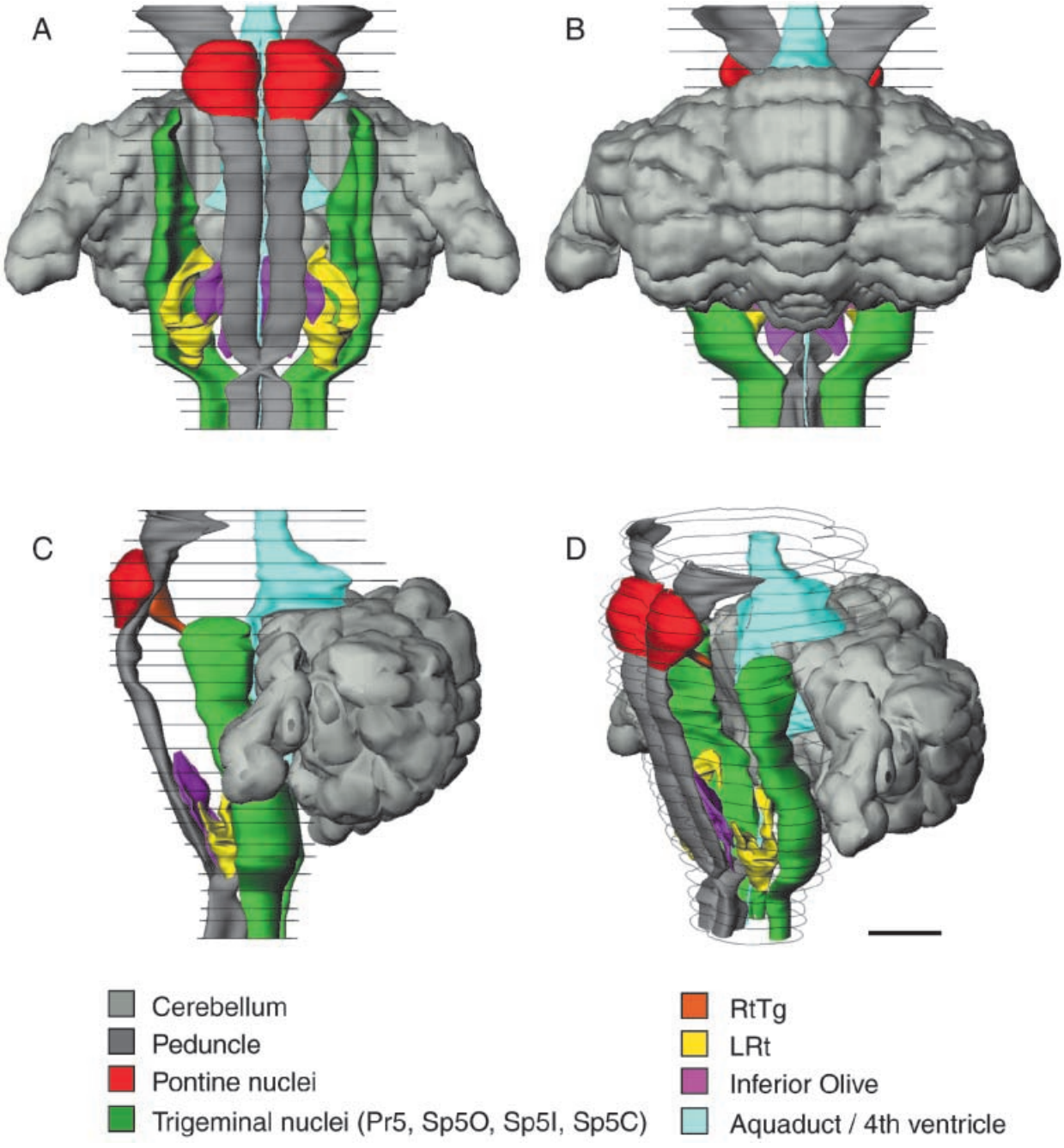

Fig. 5 Three-dimensional reconstruction of the brain stem, cerebellum, and main sensory precerebellar nuclei, shown in views from ventral (**A**), dorsal (**B**), lateral (**C**), and oblique lateral (D). The outer surface of the brain stem is represented by contour lines, and the outer boundaries of the precerebellar nuclei, the peduncle, and the cerebellum are represented by solid surfaces. The left half of the cerebellar reconstruction is a mirror copy of the right half. Programme Micro3D was used to visualise the individual components of the reconstruction separately or in different combinations. *LRt* lateral reticular nucleus; *RtTg* reticulotegmental nucleus of the pons; *Pr5* principal sensory trigeminal nucleus; *Sp5C* spinal trigeminal nucleus, caudal part; *Sp5I* spinal trigeminal nucleus, interpolar part; *Sp5O* spinal trigeminal nucleus, oral part. *Bar* 2 mm

dorsal and ventral extents of t he nuclear complex were also defined cytoarchitectonically. The boundaries rostrally (at the 'top' of Pr5), medially (at all levels), and caudally (at the transition from Sp5I to Sp5C), are more difficult to define cytoarchitectonically. Other landmarks were therefore used to position the rostral, medial, and caudal sides of the bounding box. The rostral side was arbitrarily placed at the level of the first transverse section (from rostral) containing the characteristic magnocellular cells of the trigeminal motor nucleus (Fig. 3D, D'). This level is close to the cytoarchitectonically defined 'top' of Pr5. The medial side of the bounding box was set to the midsagittal plane, and t he caudal side at the level of the first transverse section (from caudal)

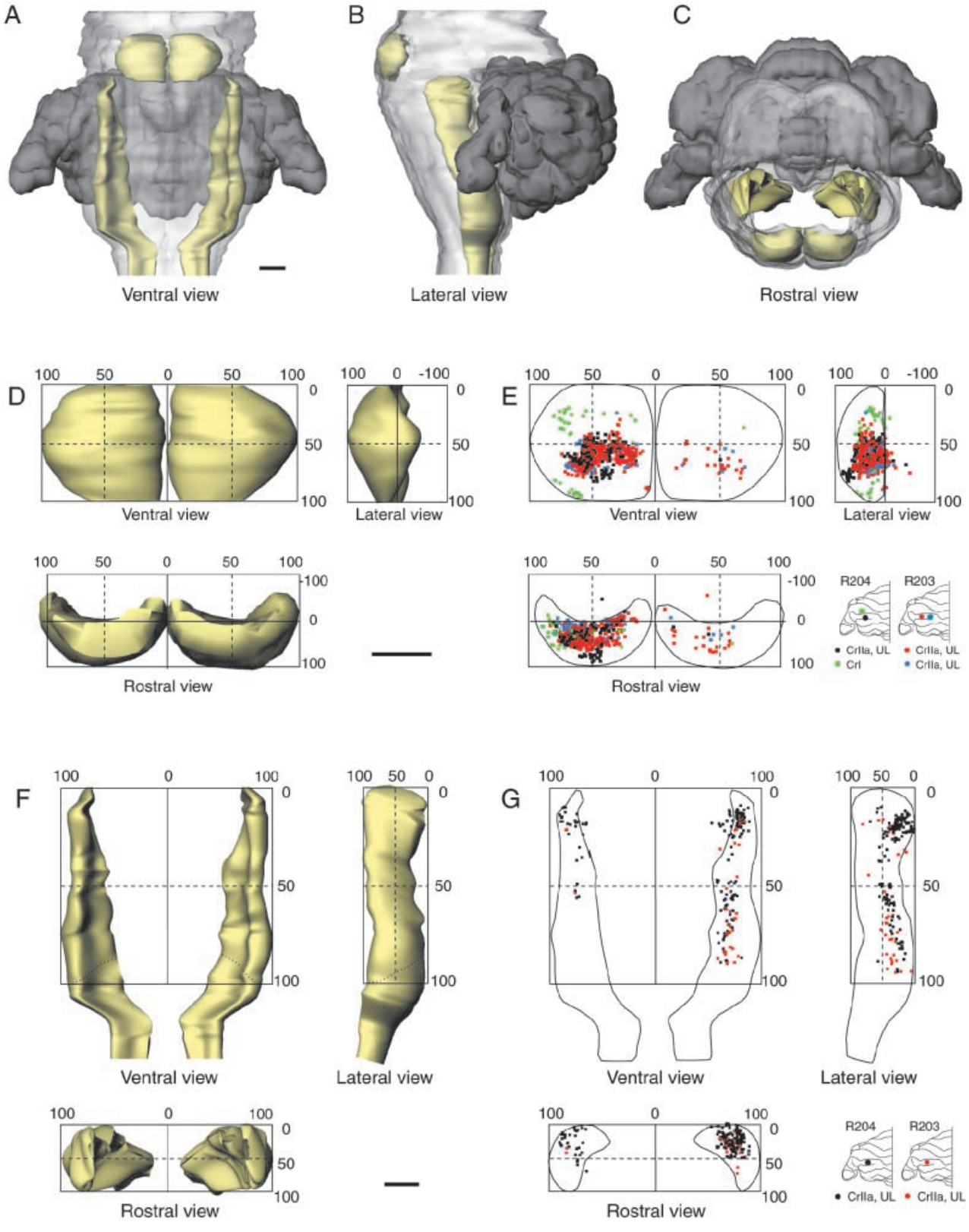
A
B
C
Ventral view
Lateral view
Rostral view
D
E
F
G
100 50 0 50 100
100 0 -100
0
50
100
-100
Ventral view
Lateral view
Rostral view
R204
R203
CrIIa, UL
CrI
CrIIa, UL
CrIIa, UL

containing cells (belonging to SP5I) between the gelatinous layer of the Sp5C and the spinal trigeminal tract. Figure 3F' shows the section adjacent and caudal to this level, with the gelatinous layer of the Sp5C neighbouring the spinal trigeminal tract.

Importing and combining data in the internal coordinate systems

The internal coordinate systems and data presentation diagrams for pontine and trigeminal sensory nuclei, as defined above, are useful for superimposing distribution data, such as neural tracing data, from different animals. First, the internal coordinate systems were applied to each data set. Data were then directly superimposed. To compensate for individual differences in size among animals, it is possible to scale (stretch or compress) the internal coordinate systems along one or more axis, to fit an average size (see Leergaard et al. 2000b), or to fit the size of any chosen template. In the present experimental material, inter-individual differences were negligible and the cases superimposed without scaling. The experimental results obtained in the present study were also compared with previously published 3-D data sets describing the distribution of terminal fields of corticopontine fibres arising in the upper lip representation of the primary somatosensory cortex (Fig. 8). These data were downloaded from a neuroinformatics data repository at http://www.nesys.uio.no/Database (see also, http://www.cerebellum.org/), and aligned with the present experimental results.

To further exploit data presented in our internal coordinate systems for other types of experiments, it appears useful to translate the 3-D coordinates from the internal nuclear coordinate systems to standard stereotaxic 3-D coordinates. In the mediolateral dimension, coordinates may be translated directly, whereas in the dorsoventral and rostrocaudal dimensions, coordinates must be corrected for different orientation of the coordinate systems. By applying the internal pontine coordinate system to a figure from the stereotaxic atlas of Paxinos and Watson (1998), using the same criteria as described above, it is possible to translate 3-D coordinates between the two systems (Fig. 7). A similar approach may be used for the trigeminal coordinate system.

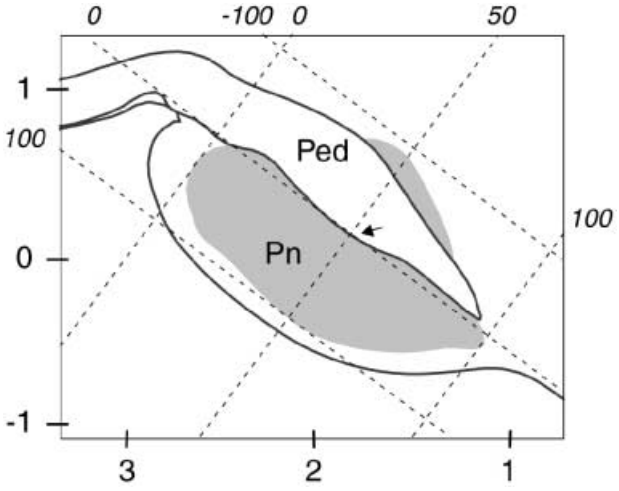

Fig. 7 Line drawing of a sagittal section through the pontine nuclei and peduncle based on the stereotaxic atlas of Paxinos and Watson (1998; lateral level 1.40 mm), shown together with the internal coordinate system for the pontine nuclei. The x-axis indicates rostrocaudal position in millimetres relative to the interaural line, while the y-axis indicates dorsoventral position relative to the interaural line. The internal pontine coordinate system is indicated by *dotted lines* that are oriented in relation to the long axis of the brain stem at the level of the pons. The rostral, ventral, and caudal boundaries of the coordinate system are adjusted to touch the boundaries of the pontine nuclei, and the dorsal boundary is defined indirectly by adjusting the centre-point (*arrow*) to touch the ventral surface of the peduncle. The figure allows translation of rostrocaudal and dorsoventral coordinates between the two coordinate systems. Mediolateral levels are identical in the two systems

◀ **Fig. 6A–G** The pontine and the trigeminal coordinate systems with imported experimental data. **A–C** Computer-generated reconstruction of the brain stem and cerebellum viewed from ventral (**A**), lateral (**B**), and rostral (**C**). The external surface of the brain stem is represented as a transparent surface. The cerebellum is represented as a solid grey surface. The outer boundaries of the pontine nuclei and sensory trigeminal nuclei are represented as solid, bright yellow surfaces. **D, F** Reconstruction of the pontine nuclei (**D**) and the sensory trigeminal nuclei (**F**) shown with angles of view from ventral, rostral (along the long axis of the respective nuclei, see Fig. 1), and lateral. The internal coordinate systems are established by adjusting a cuboid bounding box to the defined nuclear boundaries or landmarks. Frames of reference are superimposed onto the models, defined by planes tangential to the boundaries of the nuclei. Coordinate systems of relative values (%) are introduced. The coordinate system for the sensory trigeminal nuclei includes Pr5, Sp5O, and Sp5I (caudal boundary indicated by curved dotted lines in **F**). The halfway (50%) reference lines are shown as dotted lines. **E, G** Computer-generated dot maps showing the distribution of pontocerebellar (**E**) and trigeminocerebellar (**G**) projection neurons labelled after tracer implantation into crus I and IIa of the cerebellum. Experimental tracing data from two cases were superimposed. The computerized dot maps are shown as 3-D total projections. *Black dots* represent pontine neurons labelled by implantation of FR into the crown of crus IIa in case R204, and *green dots* pontine neurons labelled by implantation of FE into the crown of crus I in the same case (**E, G**). *Red dots* represent neurons labelled by implantation of FR into the crown of crus IIa in case R203, and blue dots neurons labelled by implantation of FE medially in crus IIa of the same animal (**E, G**). The size and location of the implantation sites are shown on line drawings of the left cerebellar hemispheres. Pontocerebellar projection neurons labelled by tracer implantations in the left crus IIa are distributed centrally in the right pontine nuclei, whereas neurons labelled by tracer implantation in crus I are located more rostrally and caudally. Trigeminocerebellar projection neurons labelled by tracer into the crown of the left crus IIa (putative upper lip representation, see Fig. 8), are in both cases distributed in two main clusters located dorsally in the left (ipsilateral) sensory trigeminal nuclei. *Bars* 1 mm

Mapping neuronal distribution patterns in the pontocerebellar and trigeminocerebellar systems

The experiments here reported aimed at studying the anatomic organization of the inputs to the cerebellar hemi-

spheric folium crus IIa, which is one of the most frequently studied regions of the tactile responsive regions of the rat cerebellum. Results from two cases (R203 and R204) are presented together in the same internal coordinate systems. Results from one case (R204) are also presented in combination with other, previously published, data sets. In case R203, two tracers were placed at different mediolateral locations in crus IIa (both assumed to be located in tactile facial representations, cf. Bower and Kassel 1990). In case R204 both tracers were located at the same mediolateral level (both in zebrin-positive band P5b) in adjacent folia. One tracer was placed in crus I, and the other in crus IIa. This allowed comparison of the location of precerebellar neurons within and across folia. The numbers of labelled neurons are presented in Table 1.

Implantation sites

The size of each implantation site was defined by the maximum width of dense staining at the level of the granule cell layer. The FR implantations in both cases were measured to have a diameter of 400 µm, whereas the diameters of the FE implantations were 250 µm (R203) and 300 µm (R204). None of the implantations involved white matter. In case R204, both implantation sites were located within the zebrin II-positive band P5b in crus I and crus IIa, respectively (Fig. 8). The FR implantation in crus IIa encroached upon the medial boundary of P5b+ (Fig. 8F). Using combined high-density micromapping of tactile responses in the granular layer of crus IIa and anti-zebrin II immunocytochemistry, Hallem et al. (1999) demonstrated a correspondence between the distribution of granule cell layer tactile patches and the zebrin staining pattern. They showed that the large upper lip patch on the crown of crus IIa was consistently located within the P5b+ region of zebrin labelled Purkinje cells, and that upper lip related responses continued lateral to the P5b+ region. Based on these findings, we surmise that our FR implantation in crus IIa (case R204) is located within the upper lip representation (Fig. 8G).

Pontocerebellar neurons

After tracer implantation in the putative upper lip representation on the crown of crus IIa, identified as outlined above, labelled pontine neurons were primarily located centrally in the contralateral pontine nuclei (Fig. 6E, black and red dots). A small contingent of labelled neurons was found in a mirroring ipsilateral position (Fig. 6E, ventral and rostral views). A separate tracer implantation within the same folium (FE in the medial part of crus IIa, case R203) labelled a smaller contingent of neurons in an overlapping region (Fig. 6E, blue dots; see also Table 1). In this case, most of the FE labelled neurons were double-labelled for FR, suggesting that the medial parts of crus IIa receives collateral projections from upper lip related mossy fibre projections to the crown of crus IIa. In contrast, tracer implantation in the corresponding zebrin band of the neighbouring folium crus I (FE, case R204) gave rise to labelled rostral and caudal groups of pontine neurons (Fig. 6E, ventral and lateral views, green dots), predominantly located lateral to the mediolateral 50% reference line (Fig. 6E, ventral and rostral views). Thus, the pontine neurons projecting to crus I were located external to the centrally located crus IIa projecting neurons. In case R204, none of the FE labelled neurons were double-labelled for FR, indicating that crus I and crus II receive mossy fibre afferents from different subsets of pontine neurons.

The position of the FR implantation site in crus IIa of case R204, within the zebrin II-positive region P5b+, suggested that the implantation primarily involved the tactile upper lip patch at the crown of crus IIa (Fig. 8E–G; see also Hallem et al. 1999). The distribution of pontine neurons projecting to this patch was compared with the distribution of somatosensory upper lip related cerebro-pontine projections from the primary somatosensory cortex. The cerebro-pontine data (by Leergaard et al. 2000b; data available from http://www.nesys.uio.no/Database/) showed the distribution of pontine terminal fields labelled after an implantation of biotinylated dextran amine into the electrophysiologically identified upper lip representation of SI. Combined presentation in the pontine coordinate system showed marked congruence of the distribution of the cerebropontine terminal fields and the pontocerebellar neurons (Fig. 8A–C, H–M, black dots, case R204; grey dots, case R113 from Leergaard et al. 2000b). The terminal fields of the SI upper lip area were located centrally in the pontine nuclei, in a large lateral cluster and a small medial cluster interconnected by more sparsely labelled zones of labelling. The pontine neurons projecting to the putative upper lip representation of crus IIa were mostly located

Table 1 Number of labelled pontocerebellar and trigeminocerebellar cells

	R203		R204	
	No. FR cells	No. FE cells	No. FE cells	No. FE cells
Left pontine nuclei	22	5	2	1
Right pontine nuclei	274	62	143	33
Left trigeminal sensory nuclei	33	10	115	0
Right trigeminal sensory nuclei	3	0	29	0
Total	332	77	289	34

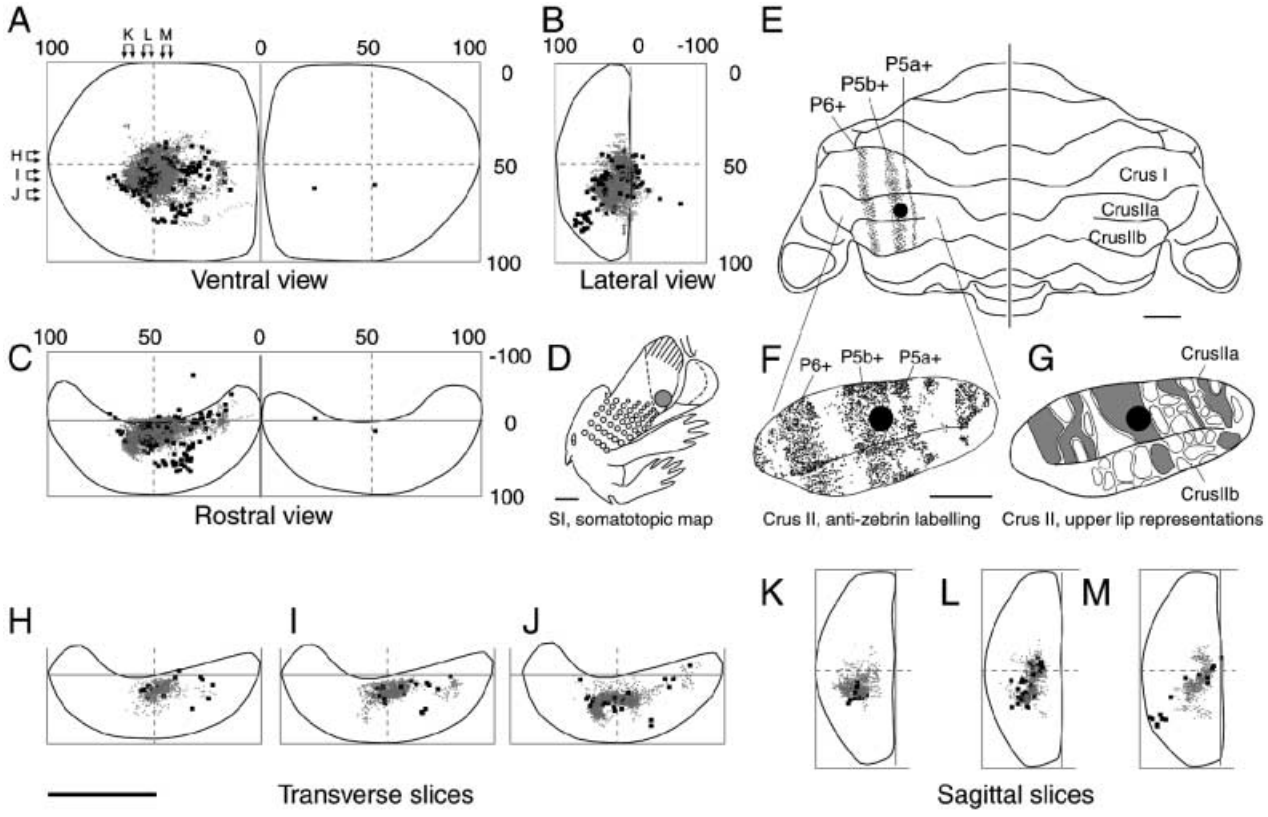

Fig. 8A–M Combined three-dimensional (3-D) map of somatosensory cerebro-pontine and ponto-cerebellar representations in the pontine nuclei. **A–C** Computer-generated 3-D dot maps (total projections) showing the distribution of corticopontine projections arising in the SI upper lip representation (*grey dots*) in combination with the distribution of pontocerebellar neurons projecting to the upper lip representation in the crown of crus IIa (*black dots*, case 204). Original 3-D reconstruction data (of corticopontine tracing results obtained after injection of biotinylated dextran amine into the upper lip representation of the primary somatosensory cortex; Leergaard et al. 2000b, their case R113) were downloaded from http://www.nesys.uio.no/database/. The data were available in Inventor file format (.iv) for use with programme Micro3D. **D** Line drawing (modified from Welker, 1971) of the SI somatotopic map. The *grey circle* indicates the position and size of the BDA injection site into the SI upper lip representation (redrawn from Leergaard et al. 2000b, their case R113, with permission). **E** Line drawing of the cerebellum, from a dorsal view. The position of the hemispheric folia crus I, crus IIa, and crus IIb are indicated on the right hemisphere. Regions in crus I and II positive to anti-zebrin II are indicated as *dotted bands* on the left hemisphere. The location of zebrin bands P5a+, P5b+, P6+ was redrawn from Hawkes and Leclerc (1987). The position and size of the FR implantation site (case R204) is indicated by a *black circle*. **F, G** Enlarged, partial view of crus II showing the relationship of the FR implantation site (*black circle*) to the zebrin-positive bands (**F**) and the tactile upper lip representation on the crown surface of crus II (**G**). *F* is a cell-by-cell reconstruction of anti-zebrin-labelled Purkinje cells in the crown of crus IIa and IIb, modified from Hallem et al.(1999), with permission. *G* shows the fractured organization of tactile representation of the crown surface of crus II, modified from Shambes et al. (1978); Bower et al. (1981); Bower and Kassel (1990), with permission. **H–M** Images of 100 µm thick selected transverse (H–I) and sagittal (K–L) slices through the reconstruction. The location of the slices is indicated by paired arrows in **A**. The anterogradely labelled corticopontine upper lip representation co-localize with the retrogradely labelled, upper lip related pontocerebellar neurons. *Bars* 1 mm

in the corresponding regions. Some neurons were located closer to the ventral surface than the pontine afferents. The selected transverse and sagittal slices reveal to advantage the high resolution of the data, and show clearly the congruence of the tactile upper lip-related pontine afferent and efferent systems.

Trigeminocerebellar neurons

Labelled trigeminocerebellar neurons were found predominantly ipsilateral to the implantation site, with a small contingent of neurons located in a mirror position (Fig. 6F, ventral and rostral views). The distribution of labelled cells after implantation of FR in the crown of crus IIa was highly similar in the two cases, both with respect to the number (Table 1) and distribution (Fig. 6G) of labelled cells. Combined presentation of the results from these two cases in the trigeminal coordinate system demonstrated that cells projecting to the upper lip related crown of crus IIa were located in the dorsal aspect of the trigeminal sensory nuclei (Fig. 6G, lateral and rostral views), with a main cluster of neurons located in the Pr5 and an elongated group of cells in the Sp5O and Sp5I (Fig. 6G, ventral and lateral views, boundaries of subnuclei not shown). Implantation of FE medially in crus IIa labelled a smaller contingent of cells, all of which were double-labelled with FR (case R203, Table 1). No cells were labelled in the trigeminal sensory nuclei after implantation of FE in crus I (case 204).

Other precerebellar nuclei

Documentation of the 3-D shape of the reticulotegmental nucleus, the lateral reticular nucleus, and the inferior olive, which may be used as a basis for future definitions of internal coordinate systems for these nuclei, is available at http://www.nesys.uio.no/Database/.

Discussion

We have prepared 3-D reconstructions of the rat brain stem with the boundaries of main precerebellar nuclei entered. The reconstructions were used as a basis for applying cyto- and myeloarchitectonically defined internal coordinate systems for the pontine nuclei and the three divisions of the trigeminal sensory nuclei projecting to the cerebellum (the Pr5, Sp5O, Sp5I). Standard diagrams for visualization of these nuclei from ventral, lateral, and rostral views, were introduced. The coordinate systems and diagrams served as a framework for investigating the distribution of identified populations of neurons and terminal fields of axons within these nuclei. Axonal tracers were injected in restricted parts of the cerebellar hemispheres, and distributions of retrogradely labelled neurons from different animals were compared following transfer of data to the same internal nuclear coordinate systems. Previously published experimental data were downloaded from a neuroinformatics data repository, presented in the same coordinate system, and compared to the new results.

The boundaries of brain stem nuclei are commonly identified with the use of cyto- and myeloarchitectonic criteria (Paxinos and Watson 1998; Swanson 1999). Other measures, based on chemoarchitecture (Paxinos et al. 1999), connectivity (Brodal 1981), electrophysiology (e.g. Bower et al. 1981), and gene expression patterns (e.g. Oberdick et al. 1998; Ragsdale and Grove 2001), provide important additional information for functional parcellation and may be introduced in future investigations, for example for subdividing of the presently studied nuclei. In the present study, we identified precerebellar nuclei on the basis of architectonic criteria in cell and/or myelin stained sections. Some cytoarchitectonic boundaries were difficult to define (e.g. the dorsal end of the pontine nuclei, and the rostral, medial, and caudal ends of the precerebellar trigeminal sensory nuclei). We bypassed this problem by using easily identifiable nearby landmarks.

Two-dimensional topographic descriptions derived from anatomic investigations depend critically on the chosen section plane. There is some variation between the frontal section planes used in stereotaxic atlases (König and Kippel 1963; Paxinos and Watson 1998; Swanson 1999), and that of our experimental material. Such variations will influence the appearance of anatomic landmarks and nuclear boundaries. The use of 3-D reconstruction allows the application of spatial reference systems that are section plane independent. The internal coordinate systems here employed may thus be used for presentation of data originating in different brains, cut in different section planes. Data sets superimposed in the same coordinate system may then be submitted to computerized re-slicing with a given slice thickness and orientation. This approach has provided a tool for distribution analyses in several recent investigations (Fig. 8; Nikundiwe et al. 1994; Leergaard et al. 1995, 2000a,b; Malmierca et al. 1998). In general, the use of computerised 3-D reconstruction facilitates the visualisation of complex anatomic structures (Malmierca et al. 1998; Leergaard et al. 2000a,b: present study) and allows various elaborate quantitative analyses (Bjaalie et al. 1991; Malmierca et al. 1998; Vassbø et al. 1999; Leergaard et al. 2000a,b). A general discussion of 3-D reconstruction approaches is provided by Bjaalie et al. (1991) and Leergaard and Bjaalie (2001).

Several recent investigations of the human brain, employing 3-D tomographic mapping methods (for reviews, see Toga and Mazziotta 1996), have attempted to create reproducible (user-independent) criteria for defining brain regions, boundaries, and spatial reference systems (Geyer et al. 2001; Toga et al. 2001, both in this issue). In the context of human brain mapping, spatial reference systems must incorporate relatively large individual structural variations. It is thus required that reference systems (to be used as frameworks for data accumulation) are deformable to fit individual brains or nuclei (Talaraich and Tournoux 1988). Population-based, probabilistic brain atlases are based on well-defined criteria for spatial matching (deformation) of individual brain maps to a normalized coordinate system (Toga and Thompson 1999; Toga et al. 2001). Such probabilistic atlases require complex algorithms to align 3-D data sets (Toga 1999).

The rat brain stem atlasing presented in this paper is less sophisticated than the human probabilistic brain atlasing approaches discussed above. In the small brains of inbred rats variations at the level of brain stem nuclei are much smaller than in the human brain. Thus, judging from a total of 80 3-D reconstructions (Leergaard et al. 1995, 2000a,b; present study) the shape and size of the pontine nuclei, as well as labelling patterns, were highly consistent. Our approach in the rat, with the use of linear scaling to fit a population-based average size (Leergaard et al. 2000b), or with direct comparison of data without scaling (present study; Leergaard et al. 2000a) is therefore well-suited for the presentation of high-resolution neural tracing data.

As demonstrated in the present (Figs. 6, 8) and previous studies (Leergaard et al. 2000a,b), the use of nuclei specific internal coordinate systems allows combined presentation of results from multiple tracing experiments. The application of standard criteria for spatial reference and data sharing via neuroanatomic data repositories further allows direct comparison of data across laboratories (as exemplified in Fig. 8). By translating the spatial distribution data to stereotaxic coordinates (Fig. 7), Eycken et al. (2000) were able to provide electrophysio-

logical support of the anatomic findings reported by Leergaard et al. (2000b).

We envision that the use of 3-D atlases, regional coordinate systems, and web-based data repositories, will play an important role in the neuroanatomy of the future. In the present paper, we have focused on the use of these tools in combination with high-resolution axonal tracing methods, to unravel detailed topography and principles of spatial organization of identified cell groups and axonal terminal fields. Numerous other methods are currently available for identification of other neural characteristics, e.g. methods for detection of neurotransmitters, enzymes, receptors, and gene products (see, e.g. Storm-Mathisen and Ottersen 1987, 1990; Brandtzaeg 1998; Danbolt et al. 1998; Petralia and Wenthold 1999). The application of microarray technique (Luo and Geschwind 2001) represents one example of a powerful new method that will allow extensive and high resolution mapping of gene expression patterns in brain sections. These and other new methods could benefit from the approaches for mapping, visualization, and analyses, outlined in the present report.

Acknowledgements Financial support was provided by The European Community Grants Bio4 CT98-0182 and QLRT-2000-02256, The Jahre Foundation, and The Research Council of Norway. We thank Richard Hawkes for providing monoclonal antibodies raised against zebrin II Purkinje-cell specific polypeptides, and Anna T. Bore and Christian Pettersen for expert technical assistance.

References

Bajo VM, Merchán MA, Malmierca MS, Nodal FR, Bjaalie JG (1999) Topographic organization of the dorsal nucleus of the lateral lemniscus in the cat. J Comp Neurol 407:349–366

Berg BG, Almaas TJ, Bjaalie JG, Mustaparta H (1998) The macroglomerular complex of the antennal lobe in the tobacco budworm moth *Heliothis virescens*: specified subdivision in four compartments according to information about biologically significant compounds. J Comp Physiol A 183:669–682

Bjaalie JG, Diggle PJ, Nikundiwe A, Karagülle T, Brodal P (1991) Spatial segregation between populations of ponto-cerebellar neurons: statistical analysis of multivariate spatial interactions. Anat Rec 231:510–523

Bjaalie JG, Daehlen M., Stensby TV (1997a) Surface modelling from biomedical data. In: Daehlen M and Tveito A (eds) Numerical methods and software tools in industrial mathematics. Birkhauser, Boston, pp 9–26

Bjaalie JG, Sudbø J, Brodal P (1997b) Corticopontine terminal fibres form small scale clusters and large scale lamellae in the cat. Neuroreport 8:1651–1655

Bower JM, Kassel J (1990) Variability in tactile projection patterns to cerebellar folia crus IIA of the Norway rat. J Comp Neurol 302:768–778

Bower JM, Beermann DH, Gibson JM, Shambes GM, Welker W (1981) Principles of organization of a cerebro-cerebellar circuit. Micromapping the projections from cerebral (SI) to cerebellar (granule cell layer) tactile areas of rats. Brain Behav Evol 18:1–18

Brandtzaeg P (1998) The increasing power of immunohistochemistry and immunocytochemistry. J Immunol Methods 216:49–67

Brodal A (1981) Neurological anatomy in relation to clinical medicine. Oxford University Press, Oxford

Chicurel M (2000) Databasing the brain. Nature 406:822–825

Danbolt NC, Lehre KP, Dehnes Y, Chaudhry FA, Levy LM (1998) Localization of transporters using transporter-specific antibodies. Methods Enzymol 296:388–407

De Schutter E, Bjaalie JG (2001) Coding in the granular layer of the cerebellum. Prog Brain Res 130:279–296

Eycken A, Bjaalie JG, Volny-Luraghi A, De Schutter E (2000) Electrophysiological study of the rat pontine nuclei. Eur J Neurosci 12:189.09 (Abstr.)

Geyer S, Schleicher A, Schormann T, Mohlberg H, Bodegård A, Roland PE, Zilles K (2001) Integration of microstructural and functional aspects of human somatosensory areas 3a, 3b, and 1 on the basis of a computerized brain atlas. Anat Embryol 204:351–366

Glover JC (1995) Retrograde and anterograde axonal tracing with fluorescent dextran-amines in the embryonic nervous system. Neuroscience Protocols, 95-030-01-01-13

Glover JC, Petursdottir G, Jansen JK (1986) Fluorescent dextran-amines used as axonal tracers in the nervous system of the chicken embryo. J Neurosci Methods 18:243–254

Hallem JS, Thompson JH, Gundappa-Sulur G, Hawkes R, Bjaalie JG, Bower JM (1999) Spatial correspondence between tactile projection patterns and the distribution of the antigenic Purkinje cell markers anti-zebrin I and anti-zebrin II in the cerebellar folium crus IIA of the rat. Neuroscience 93:1083–1094

Hawkes R, Leclerc N (1986) Immunocytochemical demonstration of topographic ordering of Purkinje cell axon terminals in the fastigial nuclei of the rat. J Comp Neurol 244:481–491

Hawkes R, Leclerc N (1987) Antigenic map of the rat cerebellar cortex: the distribution of parasagittal bands as revealed by monoclonal anti-Purkinje cell antibody mabQ113. J Comp Neurol 256:29–41

Koslow SH (2000) Should the neuroscience community make a paradigm shift to sharing primary data? Nat Neurosci 3:863–865

Köbbert C, Apps R, Bechmann I, Lanciego JL, Mey J, Thanos S (2000) Current concepts in neuroanatomical tracing. Prog Neurobiol 62:327–351

König JFR, Kippel RA (1963) The rat brain. A stereotaxic atlas of the forebrain and lower parts of the brain stem. Williams and Wilkins, Baltimore

Leergaard TB, Bjaalie JG (1995) Semi-automatic data aquisition for quantitative neuroanatomy. MicroTrace – computer programme for recording of the spatial distribution of neuronal populations. Neurosci Res 22: 231–243

Leergaard TB, Bjaalie JG (2001) Architecture of sensory map transformations: axonal tracing in combination with 3-D reconstruction, geometric modeling, and quantitative analyses. In: Ascoli G (ed): Computational neuroanatomy: principles and methods. Humana Press (in press)

Leergaard TB, Lakke EA, Bjaalie JG (1995) Topographical organization in the early postnatal corticopontine projection: a carbocyanine dye and 3-D computer reconstruction study in the rat. J Comp Neurol 361:77–94

Leergaard TB, Alloway KD, Mutic JJ, Bjaalie JG (2000a) Three-dimensional topography of corticopontine projections from rat barrel cortex: correlations with corticostriatal organization. J Neurosci 20:8474–8484

Leergaard TB, Lyngstad KA, Thompson JH, Taeymans S, Vos BP, De Schutter E, Bower JM, Bjaalie JG (2000b) Rat somatosensory cerebropontocerebellar pathways: spatial relationships of the somatotopic map of the primary somatosensory cortex are preserved in a three-dimensional clustered pontine map. J Comp Neurol 422:246–266

Lehre KP, Levy LM, Ottersen OP, Storm-Mathisen J, Danbolt NC (1995) Differential expression of two glial glutamate transporters in the rat brain: quantitative and immunocytochemical observations. J Neurosci 15:1835–1853

Luo Z, Geschwind DH (2001) Microarray applications in neuroscience. Neurobiol Dis 8:183–193

Malmierca MS, Rees A, Le Beau FE, Bjaalie JG (1995) Laminar organization of frequency-defined local axons within and between the inferior colliculi of the guinea pig. J Comp Neurol 357:124–144

Malmierca MS, Leergaard TB, Bajo VM, Bjaalie JG, Merchan MA (1998) Anatomic evidence of a three-dimensional mosaic pattern of tonotopic organization in the ventral complex of the lateral lemniscus in Cat. J Neurosci 18:10603–10618

Middleton FA, Strick PL (2001) Cerebellar projections to the prefrontal cortex of the primate. J Neurosci 21:700–712

Mihailoff GA, McArdle CB, Adams CE (1981) The cytoarchitecture, cytology, and synaptic organization of the basilar pontine nuclei in the rat. I. Nissl and Golgi studies. J Comp Neurol 195:181–201

Mihailoff GA, Lee H, Watt CB, Yates R (1985) Projections to the basilar pontine nuclei from face sensory and motor regions of the cerebral cortex in the rat. J Comp Neurol 237:251–263

Newman DB and Ginsberg CY (1992) Brainstem reticular nuclei that project to the cerebellum in rats: a retrograde tracer study. Brain Behav Evol 39:24–68

Nikundiwe AM, Bjaalie JG, Brodal P (1994) Lamellar organization of pontocerebellar neuronal populations. A multi- tracer and 3-D computer reconstruction study in the cat. Eur J Neurosci 6:173–186

Oberdick J, Baader SL, Schilling K (1998) From zebra stripes to postal zones: deciphering patterns of gene expression in the cerebellum. Trends Neurosci 21:383–390

Panto MR, Cicirata F, Angaut P, Parenti R, Serapide F (1995) The projection from the primary motor and somatic sensory cortex to the basilar pontine nuclei. A detailed electrophysiological and anatomical study in the rat. J Hirnforsch 36:7–19

Paxinos G, Watson C (1998) The rat brain in stereotaxic coordinates. Academic Press, San Diego

Paxinos G, Carrive P, Wang H, Wang P-Y (1999) Chemoarchitectonic atlas of the rat brainstem. Academic Press, San Diego

Petralia RS, Wenthold RJ (1999) Immunocytochemistry of NMDA receptors. Methods Mol Biol 128:73–92

Phelan KD, Falls WM (1989) An analysis of the cyto- and myeloarchitectonic organization of trigeminal nucleus interpolaris in the rat. Somatosens Mot Res 6:333–366

Ragsdale CW, Grove EA (2001) Patterning the mammalian cerebral cortex. Curr Opin Neurobiol 11:50–58

Reiner A, Veenman CL, Medina L, Jiao Y, Del Mar N, Honig MG (2000) Pathway tracing using biotinylated dextran amines. J Neurosci Methods 103:23–37

Ruigrok TJH, Cella F (1995) Precerebellar nuclei and red nucleus. In: Paxinos G (ed): The rat nervous system. Academic Press, San Diego, pp 277–308

Schmahmann JD, Doyon J, McDonald D, Holmes C, Lavoie K, Hurwitz AS, Kabani N, Toga A, Evans A, Petrides M (1999) Three-dimensional MRI atlas of the human cerebellum in proportional stereotaxic space. Neuroimage 10:233–260

Schwarz C, Thier P (1996) Comparison of projection neurons in the pontine nuclei and the nucleus reticularis tegmenti pontis of the rat. J Comp Neurol 376:403–419

Shambes GM, Gibson JM, Welker W (1978) Fractured somatotopy in granule cell tactile areas of rat cerebellar hemispheres revealed by micromapping. Brain Behav Evol 15:94–140

Storm-Mathisen J, Ottersen OP (1987) Tracing of neurons with glutamate or gamma-aminobutyrate as putative transmitters. Biochem Soc Trans 15:210–213

Storm-Mathisen J, Ottersen OP (1990) Immunocytochemistry of glutamate at the synaptic level. J Histochem Cytochem 38: 1733–1743

Svanevik M, Leergaard TB, Bjaalie JG (2000) Neuroinformatics database for visualisation of three-dimensional cerebro-cerebellar tracing data. Eur J Neurosci 12:64.27

Swanson LW (1995) Mapping the human brain: past, present, and future. Trends Neurosci 18:471–474

Swanson LW (1999) Brain Maps: Structure of the rat brain. Elsevier, Amsterdam

Swanson LW (2000) A history of neuroanatomical mapping. In: Toga AW, Mazziotta JC (eds) Brain mapping. The systems. Academic Press, San Diego, pp 77–109

Talaraich J, Tournoux P (1988) Co-planar stereotaxic atlas of the human brain. 3-dimensional proportional system: an approach to cerebral imaging (Translated by Mark Rayport). Thieme, New York

Tang Y, Rampin O, Giuliano F, Ugolini G (1999) Spinal and brain circuits to motoneurons of the bulbospongiosus muscle: retrograde transneuronal tracing with rabies virus. J Comp Neurol 414:167–192

Thompson JH, Lyngstad KA, Bjaalie JG, Bower JM (1995) Perioral regions of somatosensory cortex project to corresponding cerebellar regions through spatially restricted domains within the pontine nuclei. Soc Neurosci Abstr 21:467.12

Thompson PM, MacDonald D, Mega MS, Holmes CJ, Evans AC, Toga AW (1997) Detection and mapping of abnormal brain structure with a probabilistic atlas of cortical surfaces. J Comput Assist Tomogr 21:567–581

Thompson PM, Woods RP, Mega MS, Toga AW (2000) Mathematical/computational challenges in creating deformable and probabilistic atlases of the human brain. Hum Brain Mapp 9:81–92

Toga A (1999) Brain warping. Academic Press, San Diego

Toga AW, Mazziotta JC (1996) Brain mapping. The methods. Academic Press, San Diego

Toga AW, Thompson P (1999) An introduction to brain warping. In: Toga AW (ed) Brain wharping. Academic Press, San Diego, pp 1–26

Toga AW, Thompson PM, Mega MS, Narr KL, Blanton RE (2001) Probabalistic approaches for atlasing normal and disease-specific brain variability. Anat Embryol 204:267–282

Torigoe Y, Blanks RHI, Precht W (1986) Anatomical studies on the nucleus reticularis tegmenti pontis in the pigmented rat. II. Subcortical afferents demonstrated by the retrograde transport of horseradish peroxidate. J Comp Neurol 243:88–105

Ugolini G (1995) Specificity of rabies virus as a transneuronal tracer of motor networks: transfer from hypoglossal motoneurons to connected second- order and higher order central nervous system cell groups. J Comp Neurol 356:457–480

Vassbø K, Nicotra G, Wiberg M, Bjaalie JG (1999) Monkey somatosensory cerebrocerebellar pathways: uneven densities of corticopontine neurons in different body representations of areas 3b, 1, and 2. J Comp Neurol 406:109–128

Voogd J (1995) Cerebellum. In: Paxinos G (ed) The rat nervous system. Academic Press, San Diego, pp 309–352

Waite PM, Tracey DJ (1995) Trigeminal sensory system. In: Paxinos G (ed) The rat nervous system. Academic Press, San Diego, pp 705–725

Welker C (1971) Microelectrode delineation of fine grain somatotopic organization of (SmI) cerebral neocortex in albino rat. Brain Res 26:259–275

Wiesendanger R, Wiesendanger M (1982) The corticopontine system in the rat. II. The projection pattern. J Comp Neurol 208 :227–238

Woelcke M (1942) Eine neue Methode der Markscheidenfarbung. J Psychol Neurol 51:199–202